CHAPTER III

THE DEPOSITION SYSTEM FOR CIGS THIN FILMS

In this chapter, we will give the basic technique of evaporation process and the detail of our co-evaporation deposition system which was developed to fabricate the CIGS films in this research at SPRL.

3.1 Evaporation Process

3.1.1 Introduction

Physical vapor deposition (PVD) technology consists of the evaporation and sputtering techniques, which are used to deposit films. All deposition processes from these techniques take place in a vacuum system. The thickness of the films can vary from angstroms to millimeters. The objective of the deposition processes is to controllably transfer atoms from a source to a substrate where film formation and growth proceed atomistically. In the evaporation technique, the atoms are removed from the source by thermal means, whereas in the sputtering technique they are dislodged from the surface of the source (solid target) through impact of gaseous ions [34, 35].

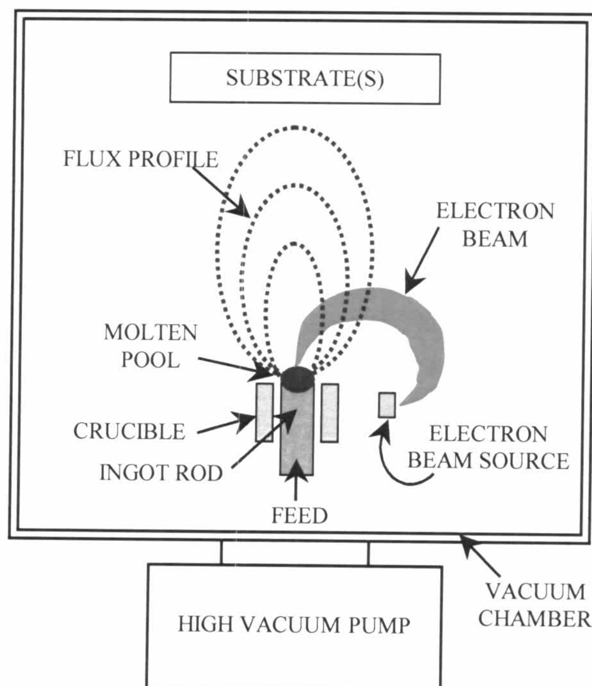

Figure 3.1: Schematic diagram of an evaporation system using electron beam heating.

The uses of these techniques range over a wide variety of applications from decorative to utilitarian, covering significant segments of the engineering, chemicals, nuclear, microelectronics and related industries.

A schematic diagram of an evaporation system is shown in Fig 3.1. Typically, it consists of an evaporation source (which can be a thermally heated crucible, electron beam, laser beam, etc.) to vaporize the desired material [34,35]. The substrates are located at an appropriate distance facing the evaporation source. Evaporation is carried out in the pressure range of 10^{-5} to 10^{-8} Torr. In this pressure range, the mean free path of atoms (or molecules) of the evaporant material is very large ($5x10^{2}$ to 10^{5} cm) as compared to the source-to-substrate distance.

For a basic sputtering process, as illustrated schematically in Fig. 3.2, positive gas ions (usually argon ions) produced in a glow discharge (gas pressure 20 to 150 mTorr) bombard a target material (also called the cathode) dislodging group of atoms which then transform to the vapor phase and deposit onto the substrate [35, 36].

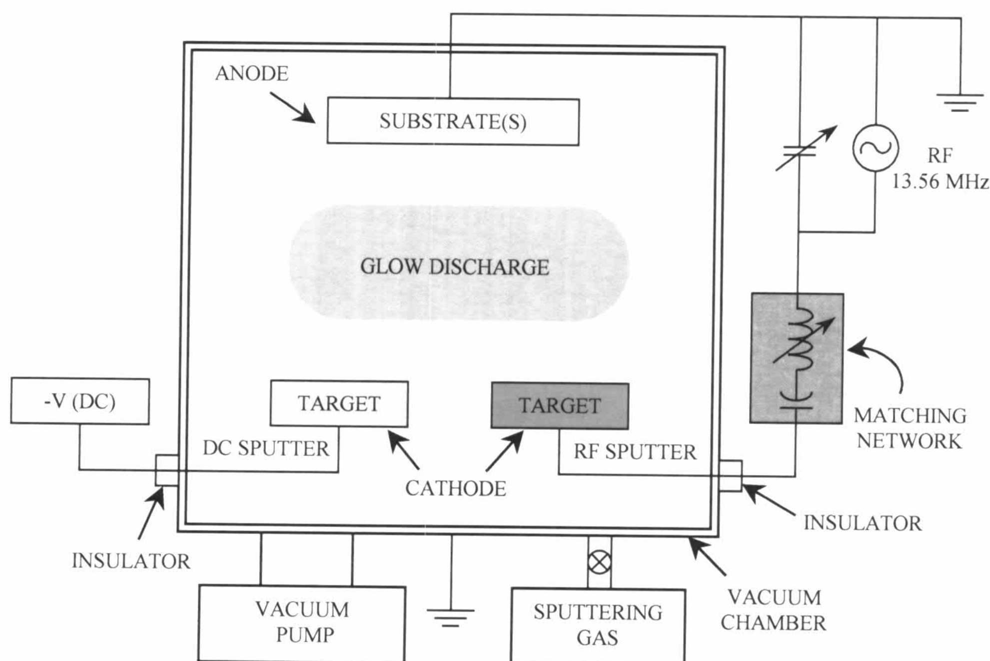

Figure 3.2: Schematic diagram of a simplified sputtering system: DC and RF.

3.1.2 Model of Film Growth in Evaporation Process

In general, all deposition processes consist of three major steps. These are shown in Fig. 3.3. More specifically, for physical vapor deposition processes, they are:

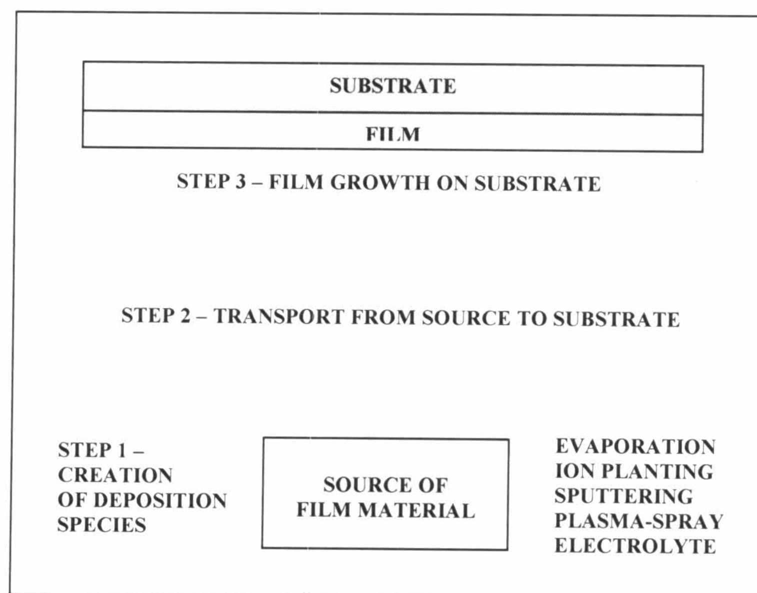

Figure 3.3: The three steps in film deposition for PVD process [36].

Step 1: Generation of the depositing species. This involves (a) a transition from condensed phase (solid or liquid) to vapor phase, and (b) for deposition of compounds, a reaction between the components of the compound, some of which may be introduced into the chamber as a gas or vapor.

Step 2: Transport of the species from source to substrate. This occurs at low partial pressures of the depositing species and the residual gas in the system. This is responsible for the line-of-sight feature typical for evaporation-deposition processes and low-pressure magnetron type sputtered deposition processes. Viscous flow occurs at higher partial pressure (20-150 mTorr) typical of diode sputter deposition. It also occurs when a substantial partial pressure of an inert gas is intentionally added in the evaporation deposition process to cause gas-scattering of the depositing species.

Step 3: Film growth on the substrate. The processes occurring on the substrate depend on the energy of the incident species (which is typically

0.5 eV for evaporation and 10 to 100 eV for sputtering) and the substrate temperature. The structure, composition and residual stress in the film can be substantially changed by bombardment of the growing film by energetic ions or neutrals. These can be generated by a separate ion source, or they can be attracted to the film from the plasma by electrical biasing of the substrate/film. Thus the location of the substrate inside the plasma or outside the plasma can substantially change the nature and amount of ion bombardment.

3.1.3 Basic Theory and Mechanisms [34-36]

The evaporation technique is used to deposit materials by heating a source material under vacuum until it evaporates or sublimes. Typically, the rate of deposition can be expressed by the Hertz-Knudsen Equation,

$$\frac{1}{A}\frac{dN}{dt}=\frac{\alpha(p^*-p)}{\sqrt{2\pi mkT}} \quad , \qquad (3.1)$$

where $\frac{dN}{dt}$ is the rate of molecules evaporating from a source with surface area A,

α is the evaporation coefficient which is unity for clean surfaces and low values for contaminated surfaces,

p^* is the equilibrium vapor pressure at the evaporating surface,

p is the hydrostatic pressure acting on the surface,

m is the molecular weight of the evaporating material,

k is Boltzmann's constant,

and T is the absolute temperature.

When $\alpha = 1$ and p is zero, the maximum evaporation rate is obtained.

The film thickness can be controlled by the rate of the generated vapor material as well as the distance from source to substrate. Typically, the deposition rates depend significantly on the substrate-to-source geometry, and vary across large substrates because the effect of source-to-substrate distance on film thickness. The effect of the variation in deposition rate resulting from substrate position relative to source can be shown in film thickness distribution.

Two simple ideal sources are a small source, referred to as a point emitter, and an extended source, referred as a surface emitter, as shown in Fig. 3.4.

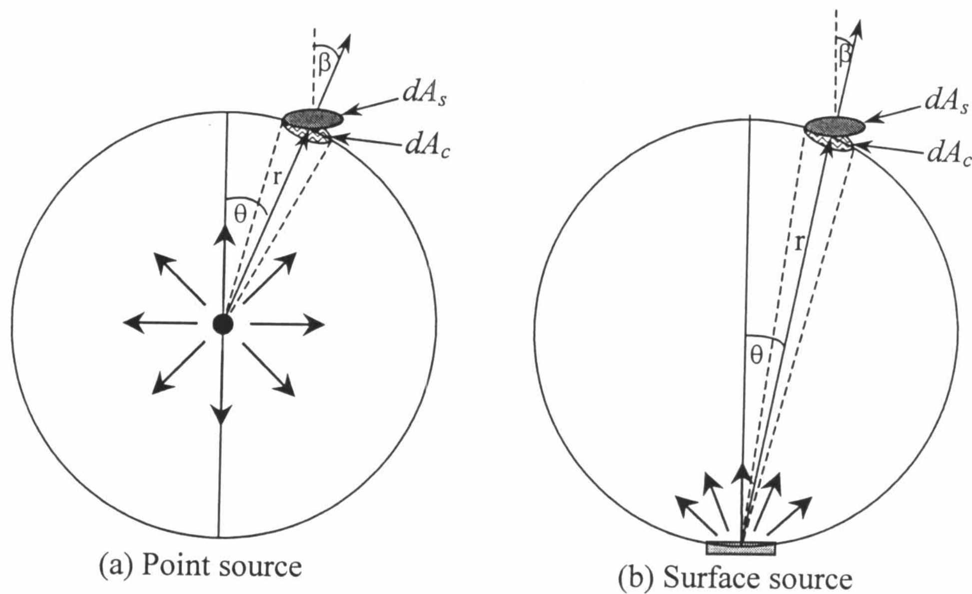

Figure 3.4: Evaporation from (a) a point source, (b) a surface source [35].

The point source can be considered as a small sphere evaporating an equal amount of material spherically in all directions. The amount of material incident on the receiving surface is equal to the amount of material passing through the solid angle subtended at the source by the surface as shown in Fig. 3.4(a). The infinitesimal amount of material received by the surface is given by

$$dM_s = CM_e d\Omega = CM_e \frac{dA_c}{r^2} = CM_e \frac{\cos\beta \, dA_s}{r^2}, \qquad (3.2)$$

where dM_s is the infinitesimal amount of material received by the surface,

M_e is the total mass evaporated from source,

C is the proportionality constant evaluated by integrating over entire receiving surface,

$d\Omega$ is the solid angle subtended at the source by the surface,

β is the angle between the normal to the surface and the line between the source and receiving surface,

dA_s is the infinitesimal receiving surface on the substrate,

dA_c is the projected area of dA_s on the surface of the sphere,

and r is the distance from the center of source to the center of receiving surface.

If the receiving surface is the entire surface of a sphere with its center at the source, then $\beta = 0$ and $dA_s = 2\pi r^2 \sin\theta \, d\theta$. Integration of Eq. (3.2) over a sphere gives

$$M_s = CM_e \int_{\theta=0}^{\pi} 2\pi \sin\theta \, d\theta = CM_e 4\pi \qquad . \qquad (3.3)$$

Since $M_e = M_s$ in the case of a sphere, then $C = \frac{1}{4\pi}$ and we obtain

$$dM_s = \frac{M_e \cos\beta \, dA_s}{4\pi r^2} \quad \text{(point source).} \qquad (3.4)$$

If the point source is replaced with a surface source as shown in Fig. 3.4(b). The surface source has emissive properties such that the amount of material evaporated at any angle is proportional to the cosine of that angle. When a molecule collides with a receiving surface plane, the angle (θ) at which it leaves the source plane is independent of the angle (β) at which it arrives the substrate.

In order to account for the directional emissive properties of the surface source, then Eq. (3.2) becomes

$$dM_s = CM_e \cos\theta \, d\Omega = CM_e \frac{\cos\theta \cos\beta \, dA_s}{r^2} \quad . \qquad (3.5)$$

In this surface source, the emission is limited to a hemisphere, and the integration of Eq. (3.5) over a hemisphere gives $C = \frac{1}{\pi}$, then Eq. (3.5) becomes

$$dM_s = \frac{M_e \cos\theta \cos\beta \, dA_s}{\pi r^2} \qquad \text{(surface source)}. \qquad (3.6)$$

Assuming the deposited film has a constant density (ρ), Eqs. (3.4) and (3.6) can be converted to an equivalent film thickness (t). Then the film thickness for point and surface sources can be written as

$$dM_s = \rho \, t \, dA_s \quad , \qquad (3.7)$$

$$t = \frac{M_e \cos\beta}{4\pi\rho r^2} \qquad \text{(point source)}, \qquad (3.8)$$

and

$$t = \frac{M_e \cos\theta \cos\beta}{\pi\rho r^2} \qquad \text{(surface source)}. \qquad (3.9)$$

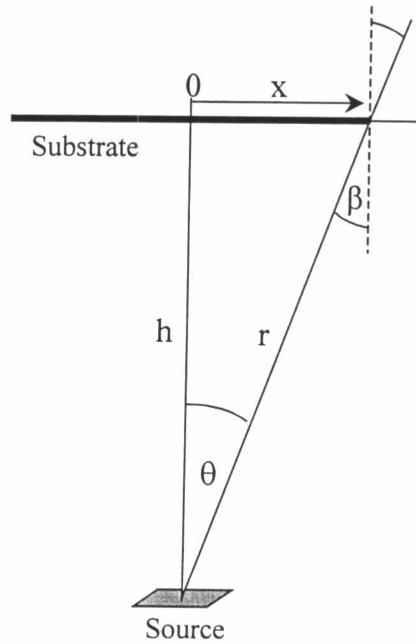

Figure 3.5: Geometry of h and x, vertical and horizontal substrate distances, respectively.

The relative thickness distribution for a point source and a surface source can be determined in terms of the position of the film relative to the source as shown in Fig 3.5. The receiving surface is a plane surface parallel to the source surface, i.e., $\theta = \beta$. The relative thickness equations are obtained by substituting $cos\,\beta = cos\,\theta = h/r$ and $r^2 = x^2 + h^2$ into Eq. (3.8) and Eg. (3.9). Here x is the horizontal distance across substrate from a point directly above or below the source, and h is the vertical distance from source to substrate.

For the point source, the thickness of deposition at some horizontal distance x from the center of the receiving surface,

$$t_x = \frac{M_e \cos\beta}{4\pi\rho r^2} = \frac{M_e h}{4\pi\rho r^3} = \frac{M_e h}{4\pi\rho\left(h^2 + x^2\right)^{3/2}} \quad . \qquad (3.10)$$

The maximum thickness (t_0) at the center of the receiving surface directly above the source occurs at $x = 0$, in which case $t_0 = \frac{M_e}{4\pi\rho h^2}$, and thus,

$$\frac{t_x}{t_0} = \left[1 + \left(\frac{x}{h}\right)^2\right]^{-3/2} \qquad \text{(point source).} \qquad (3.11)$$

Similarly, for the surface source

$$t_x = \frac{M_e \cos\theta \cos\beta}{\pi\rho r^2} = \frac{M_e h^2}{\pi\rho\left(h^2 + x^2\right)^2} \quad . \qquad (3.12)$$

When normalized to the maximum thickness in this case; $t_0 = \frac{M_e}{\pi\rho h^2}$,

$$\frac{t_x}{t_0} = \left[1 + \left(\frac{x}{h}\right)^2\right]^{-2} \qquad \text{(surface source).} \qquad (3.13)$$

3.2 The CIGS Deposition System

Generally, the device-quality chalcopyrite (CIGS) thin films are fabricated to have a final non-stoichiometric composition, lying in the immediate vicinity of the Cu_2Se-In_2Se_3 pseudobinary line (Fig. 2.1), where the chalcogen (Se) offered at over-stoichiometric concentration during the growth process. This is due to the high Se vapor pressure at the deposition temperature (> 400°C) preventing the incorporation of the additional chalcogen atoms into the lattice. Depending on the deviation of molecularity (Δm) of the elemental composition, growth processes are divided into Cu-rich ($\Delta m > 0$) and Cu-poor ($\Delta m < 0$) ones. As discussed in Section 2.1, the structural properties and the defect chemistry of the chalcopyrite phase are greatly influenced by the Δm parameter, independently of the specific film deposition method [37, 38, 39]. Sophisticated co-evaporation processes which are nowadays used for absorber layer preparation of the most efficient chalcopyrite thin film solar cells utilize this feature of the chalcopyrite compound as they switch between the Cu-rich regime (to provoke large grain sizes and good structural properties) and the In-rich regime (to avoid secondary phases in the final layer) during the growth. Such typical processes are referred to as two-stage process [33, 39].

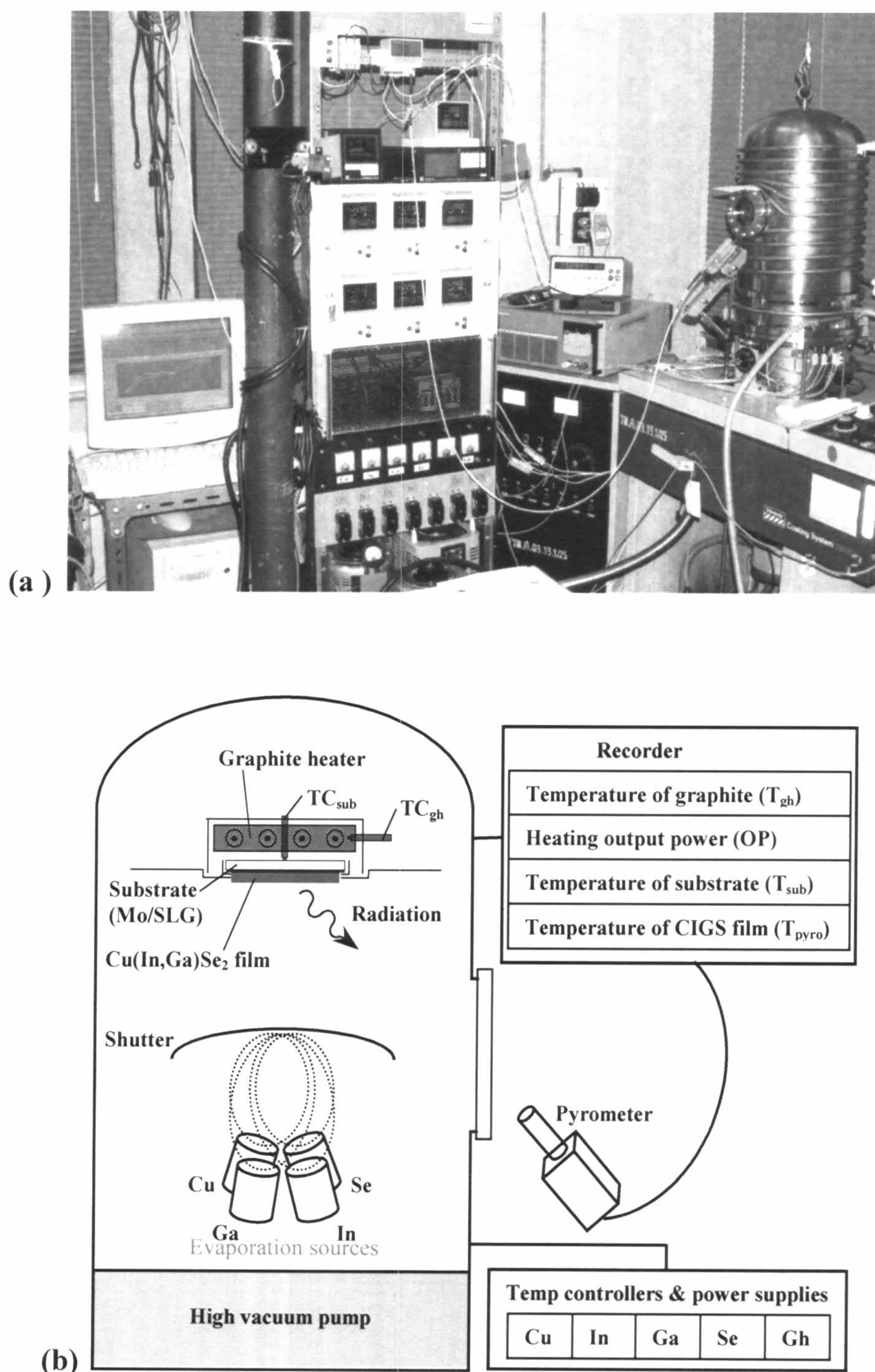

Figure 3.6: (a) Photograph of the CIGS deposition system at SPRL, (b) Schematic diagram of the multi-source co-evaporation system with the *in situ* monitoring: heating output power, pyrometer, thermocouples.

Several deposition techniques have been employed to produce the chalcopyrite thin films, e.g. single source evaporation, multi-source co-evaporation, electroplating, spray pyrolysis and reactive sputtering [40]. However, up to now the device quality CIGS material has been achieved by multi-source co-evaporation [37, 41, 42]. Therefore, the deposition system using multi-source co-evaporation technique was constructed at SPRL as shown in Fig. 3.6(a). We have also developed our two-stage growth process by simultaneously using a pyrometer, heating output power and thermocouples signal to detect the desired Cu-deficient composition or the end point detection (EPD). The schematic diagram of the evaporation system is illustrated in Fig. 3.6(b). It consists of the following: vacuum chamber, pumping station, substrate holder, graphite heater, evaporation sources, shutter, radiation shield, pyrometer and etc.

3.2.1 Vacuum Chamber and Pumping System

Our vacuum chamber (see in Fig. 3.7) is a stainless steel bell jar which has the diameter of 31 cm and the height of 65 cm. The bell jar has a view port for thermal radiation measurement from the surface of the sample. During the deposition process (typically 1 hr), the chamber wall can be heated by the thermal radiation from the substrate heater and the evaporation sources. Especially, the rubber gasket could be melted when its temperature is over 95°C. Therefore, the chamber has to add the cooling coil for closed-cycle cooling water. The conventional high vacuum pump with a cold cap baffle was used. The base pressure of the growth chamber was approximately $1x10^{-5}$ mbar

($7.6x10^{-6}$ Torr). The schematic diagram of the vacuum pumping system is illustrated in Fig. 3.8.

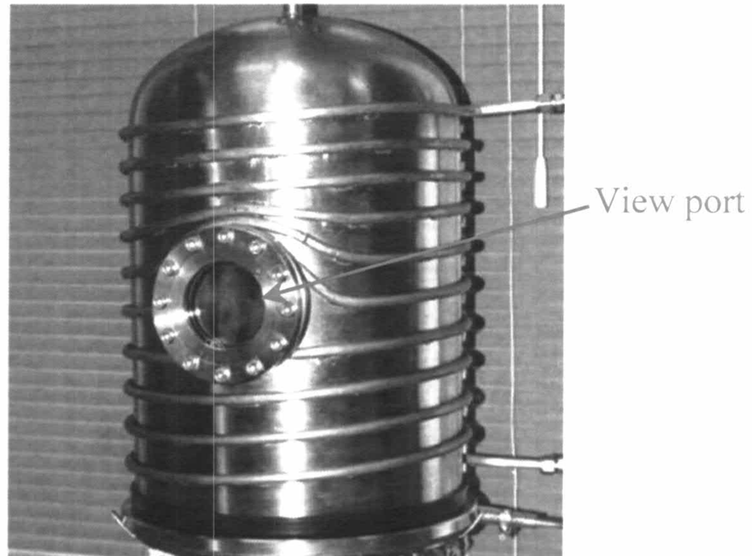

Figure 3.7: Photograph of the vacuum chamber.

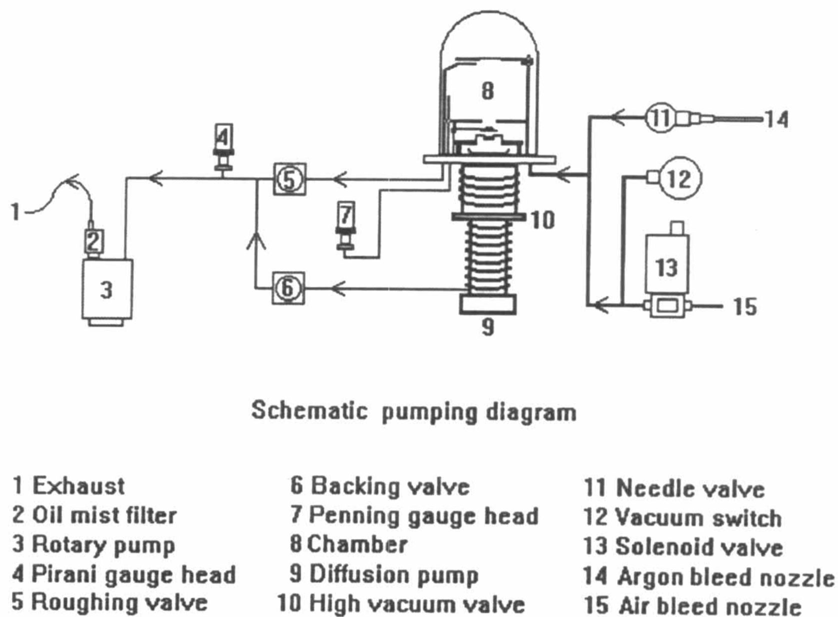

Figure 3.8: Schematic diagram of the vacuum pumping system [43].

3.2.2 Graphite Heater and Substrate Holder

A molybdenum coated soda-lime glass (Mo/SLG) substrate (2 mm thick with area 5x6 cm^2) was placed in a substrate holder which was made of molybdenum sheet (see in Fig. 3.9). The Mo/SLG substrate positioned approximately 25 cm above the sources was heated by radiation from a graphite heater. The reasons for these are to ensure uniformity of film thickness and to control the temperature over a large area of the substrate. Tantalum wires were used as the filaments for the graphite heater. The thermocouples are "in contact" with the graphite heater and the backside of the substrate. The schematic drawing of the graphite heater and the substrate is illustrated in Fig. 3.10.

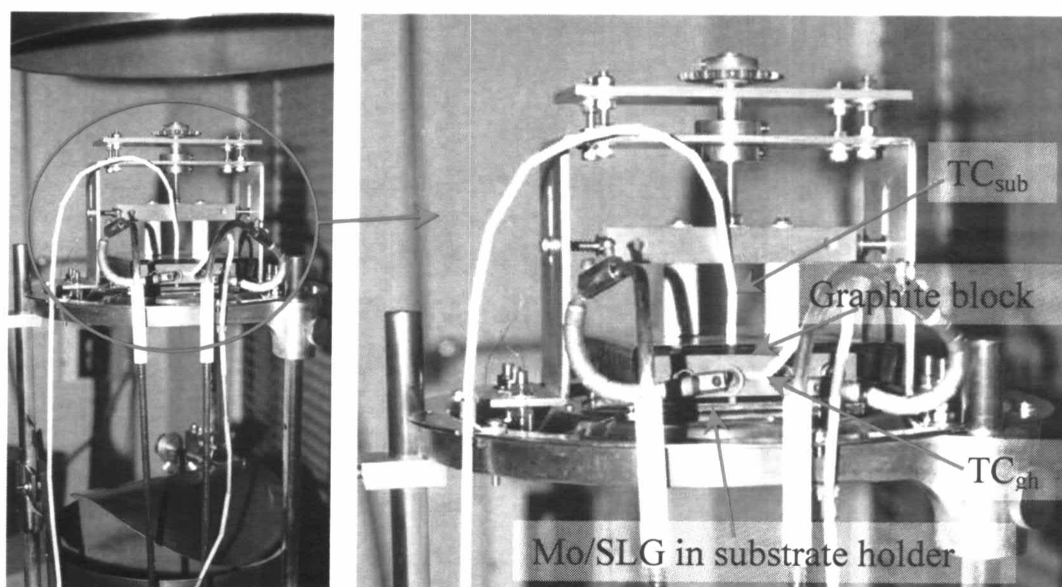

Figure 3.9: Photographs of the graphite heater and the substrate holder.

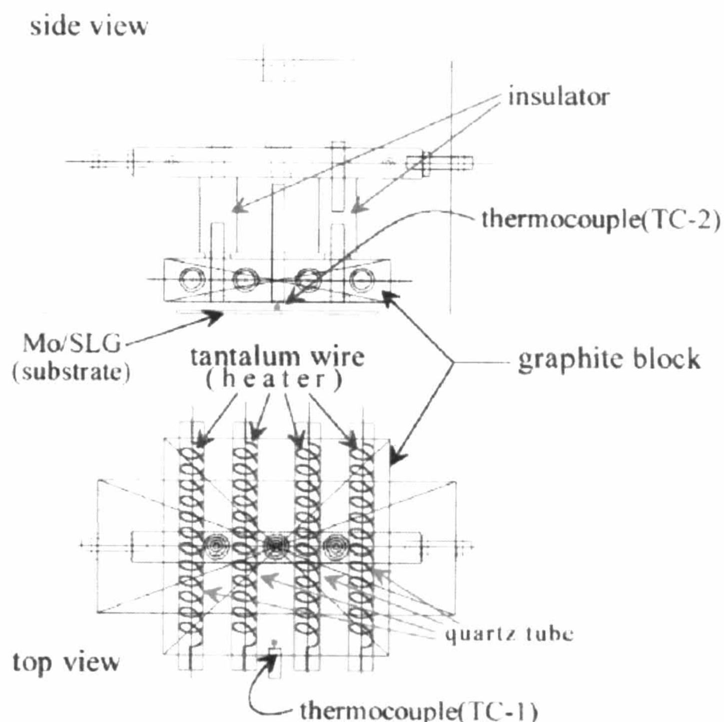

Figure 3.10: Schematic drawing of the graphite heater and the substrate.

3.2.3 Evaporation Sources (Cu, In, Ga and Se)

In general, evaporation sources are utilized for conversion of the solid or liquid evaporant to the vapor phase in vacuum. All types of evaporation sources are classified by the mode of heating. Knudsen cells (K-cells) are the most common type of evaporation source in the molecular beam epitaxy (MBE) systems. In its ideal form, a Knudsen cell is a heated cavity with an orifice small enough that it does not disturb the equilibrium vapor pressure inside. The effusion rate from the orifice then depends only on the vapor pressure of the evaporant, and not on the amount of the evaporant. However, deposition rates from idealized Knudsen cells are very small, and the orifice can become blocked [44]. Practical Knudsen cells thus have large openings to allow useful

deposition rates, but the rate varies with evaporant fill level. This can be minimized by not completely filling the cell and kept filling the evaporant to the same level. The distribution of the evaporated flux depends on the crucible shape and varies with oblique angle of the cell. Therefore, our prototypes of the evaporation sources for Cu, In, Ga and Se were completely designed and constructed as shown in Fig. 3.11.

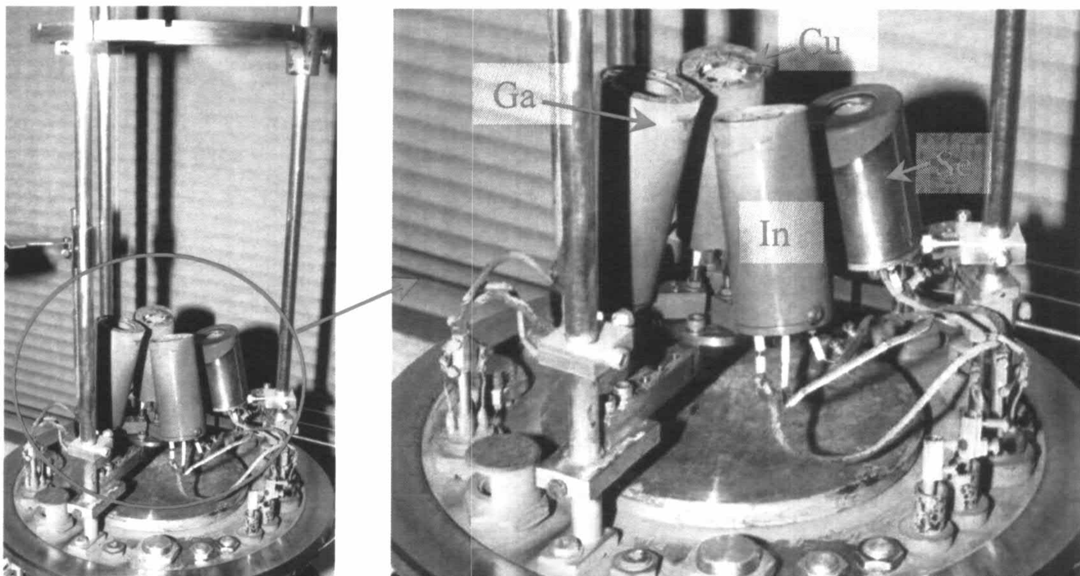

Figure 3.11: Photographs of the evaporation sources for Cu, In, Ga and Se.

For the detail of evaporation sources, we used a typical alumina (Al_2O_3) crucible for the Se source working at temperatures below 500°C and pyrolytic boron nitride (PBN) crucibles for the three metallic sources. PBN is stable to temperature as high as 1400°C, and refractory metals are not reactive even at high temperatures [44]. The heaters for each evaporation source were made from two tantalum wires (the same diameter of 0.5 mm), which were twisted and coiled to fit snugly around each crucible. The temperature of each source

was read at the bottom of the crucible by the Chromel-Alumel (K-type) thermocouple. The several layers of Mo-shield were utilized as the internal reflector for all heat radiation from the tantalum heater. Moreover, the furnace cases were constructed from stainless steel to prevent corrosion. The structure of evaporation sources is illustrated in Fig. 3.12. The properties of selective materials for the source components are shown in Table 3.1.

Figure 3.12: Photograph of the structure of evaporation sources.

Table 3.1: Properties of selective materials for the source components [45].

Name	Symbol	Melting point (°C)	Temperature (°C) Vapor pressure	
			@10^{-8} Torr	@10^{-4} Torr
Alumina	Al_2O_3	2045	-	1550
Pyrolytic Boron Nitride	PBN	2300	-	1600
Molybdenum	Mo	2610	1592	2217
Tantalum	Ta	2996	1960	2590

3.2.4 Shutter and Radiation Shield

In the vacuum chamber, the direct heat radiated from the evaporation sources and the graphite heater to the chamber wall can be reduced using the radiation shield and shutter. Other purpose of the shutter is to close the arrival fluxes at the substrate. The manual shutter can be closed and opened from outside of the chamber as shown in Fig. 3.13.

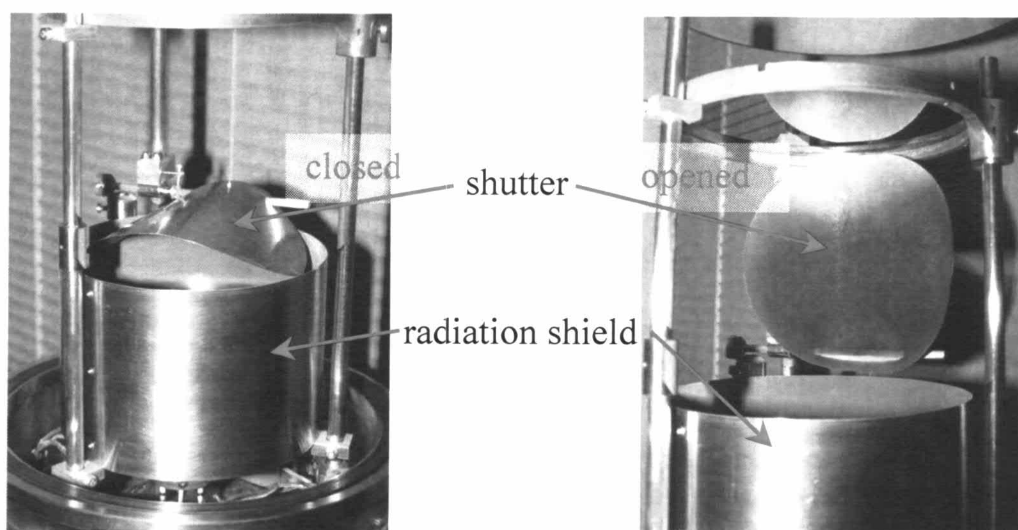

Figure 3.13: Photographs of the shutter and radiation shield.

3.2.5 Source Calibration

The purity materials (Cu, In, Ga:6N, Se:5N) were evaporated from our four Knudsen-type sources. The four evaporation sources were independently controlled by programmable proportional integral derivative (PID) temperature controllers to emit appropriate fluxes of Cu, In, Ga and Se. All evaporation sources were aligned firstly to achieve the uniform film and flux over a large area of glass substrate which has a diameter of about 21 cm. The thickness

distribution of the film on substrate were measured by the optical transmission technique using a laser beam and a photodetector (see in Fig. 3.14). Using this technique to feed back the films resulting from the source alignment, we then achieved uniform films over the substrate as shown in Fig. 3.15 (e.g. Cu film at 1030°C).

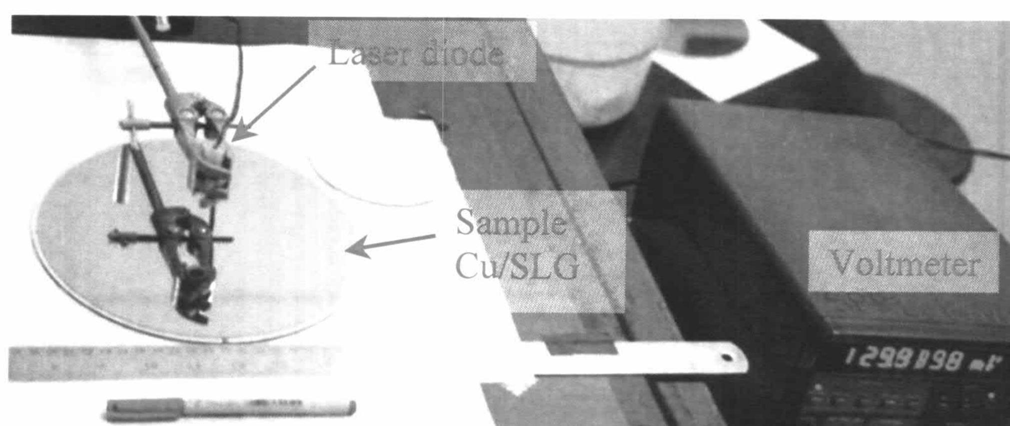

Figure 3.14: Photograph of the optical transmission measurement set-up for the thickness distribution of film on the substrate.

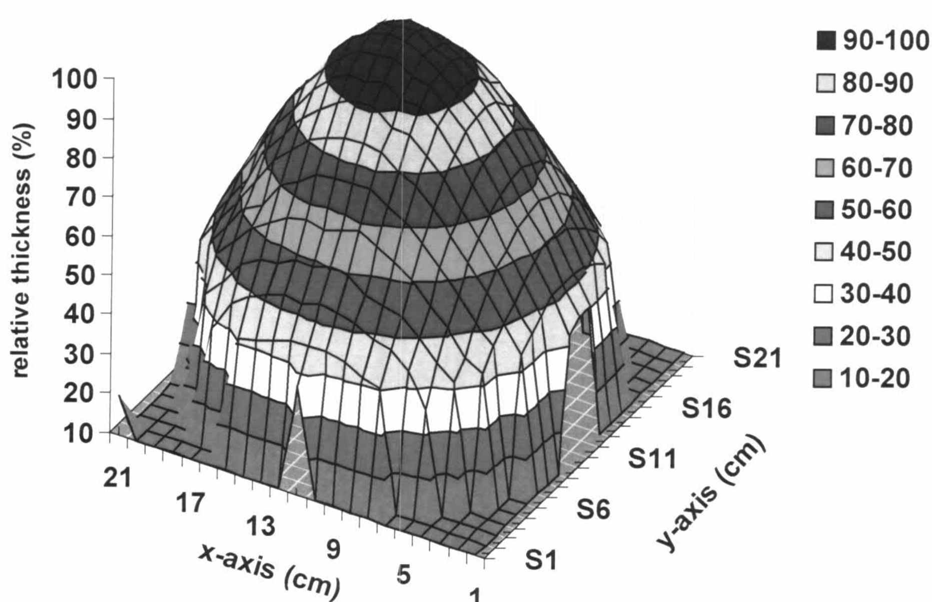

Figure 3.15: The thickness distribution of Cu film on the large area of glass substrate.

In order to obtain the relation between source temperature and deposition rate, the Quartz Crystal Monitor (QCM) was used and it was installed at the center of substrate as shown in Fig. 3.16.

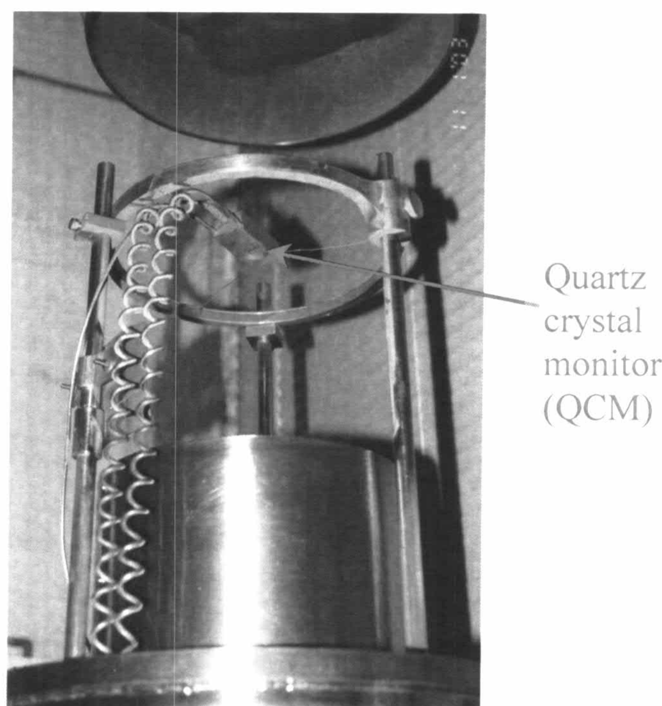

Figure 3.16: Photograph of the quartz crystal monitor at the center of substrate.

In principle, QCM utilizes the piezoelectric sensitivity of a quartz monitor crystal to added mass. The QCM uses this mass sensitivity to calculate the deposition rate and the final thickness of the deposited film. The resonance frequency induced by an a.c. field is inversely proportional to crystal thickness or added mass of the film on the crystal surface. The change in frequency of the crystal is compared to the reference frequency. This effect provides a mean of determining how much material deposited on a substrate in a vacuum system.

For our deposition system at the same background pressure, the calibration was obtained by one evaporation source at a time. Each evaporation

source was calibrated at eight or nine different temperatures in the range of working temperature. The relation between the source temperature (T) and the deposition rate (r) follows the Eq. (3.14) [46],

$$ln(r) = a \cdot \frac{1}{T} + b \qquad . \qquad (3.14)$$

Using a least-square fit method, the parameters a and b can be determined as shown in Fig. 3.17(a, b, c and d).

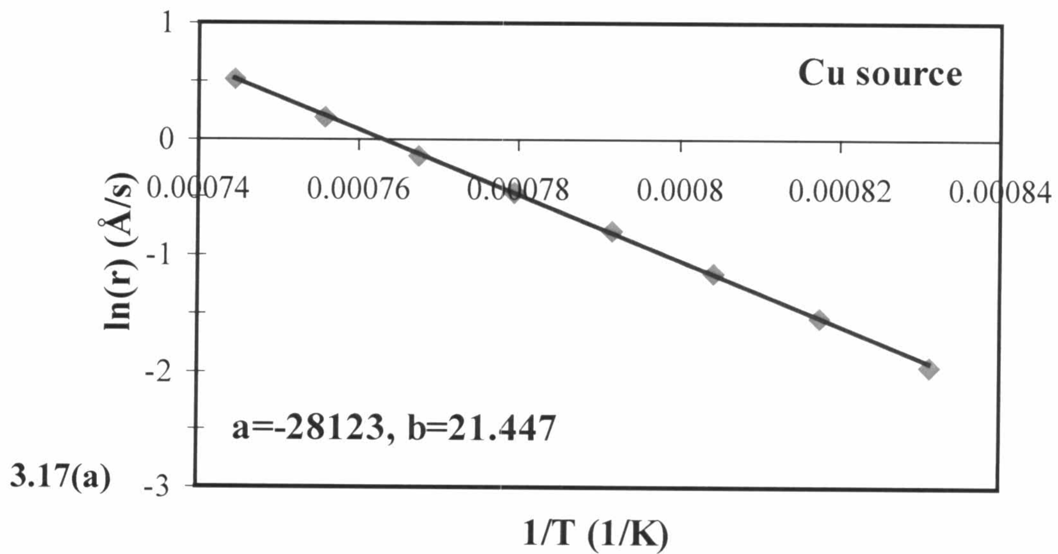

3.17(a)

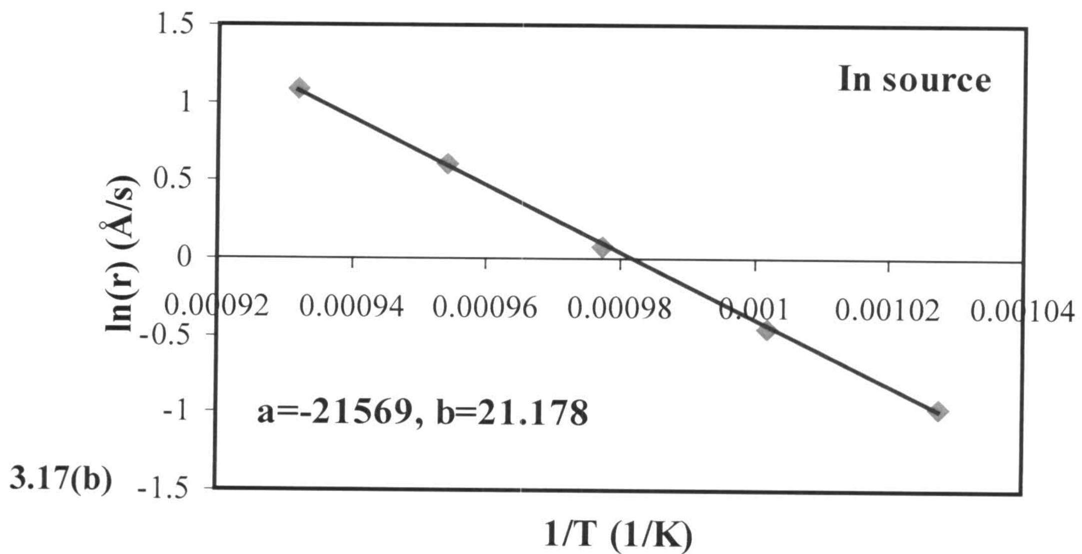

3.17(b)

3.17(c)

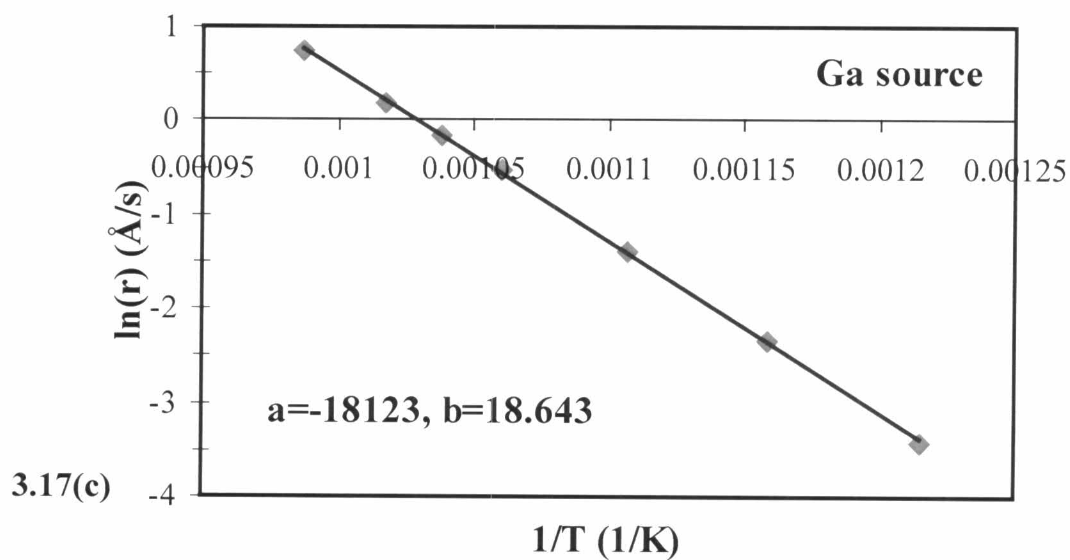

3.17(d)

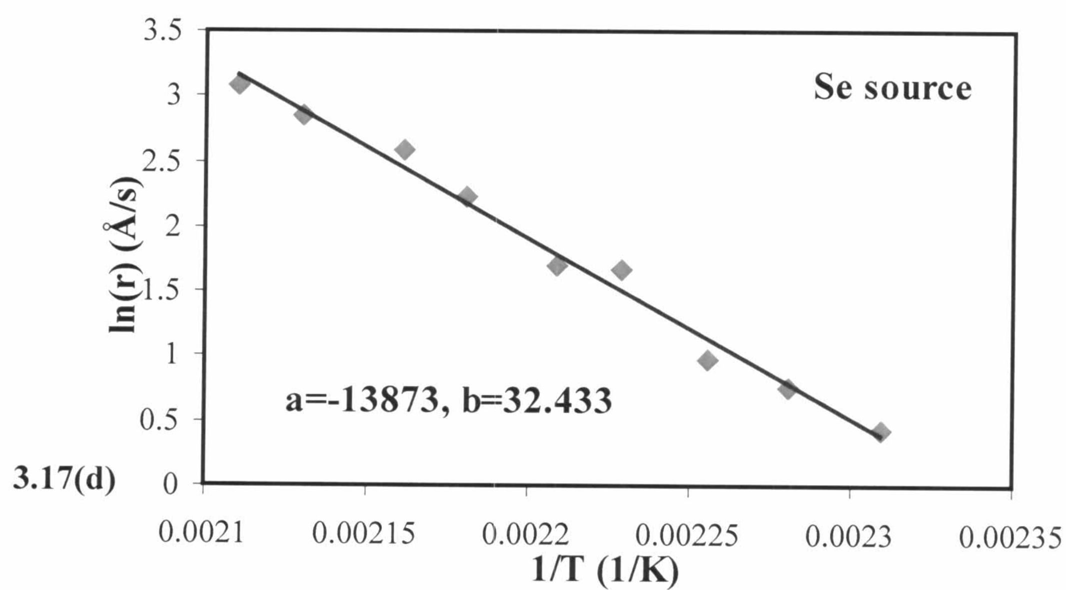

Figure 3.17: The plots of *ln(r)* versus *1/T* for (a) the Cu source, (b) the In source, (c) the Ga source and (d) the Se source.

3.2.6 Pyrometer

Using non-contact temperature measurement, the heat radiation from the front surface of the substrate was monitored by a high resolution monochromatic (InGaAs, 1.55 μm) pyrometer. This pyrometer (IR-FA) is a fiber type radiation thermometer which has a measuring range of 250 to 1000°C. It was installed on the x-y stage slide table at the view port of the chamber. The pyrometer then was focused to the center of the substrate surface by the built-in laser guided device as shown in Fig. 3.18.

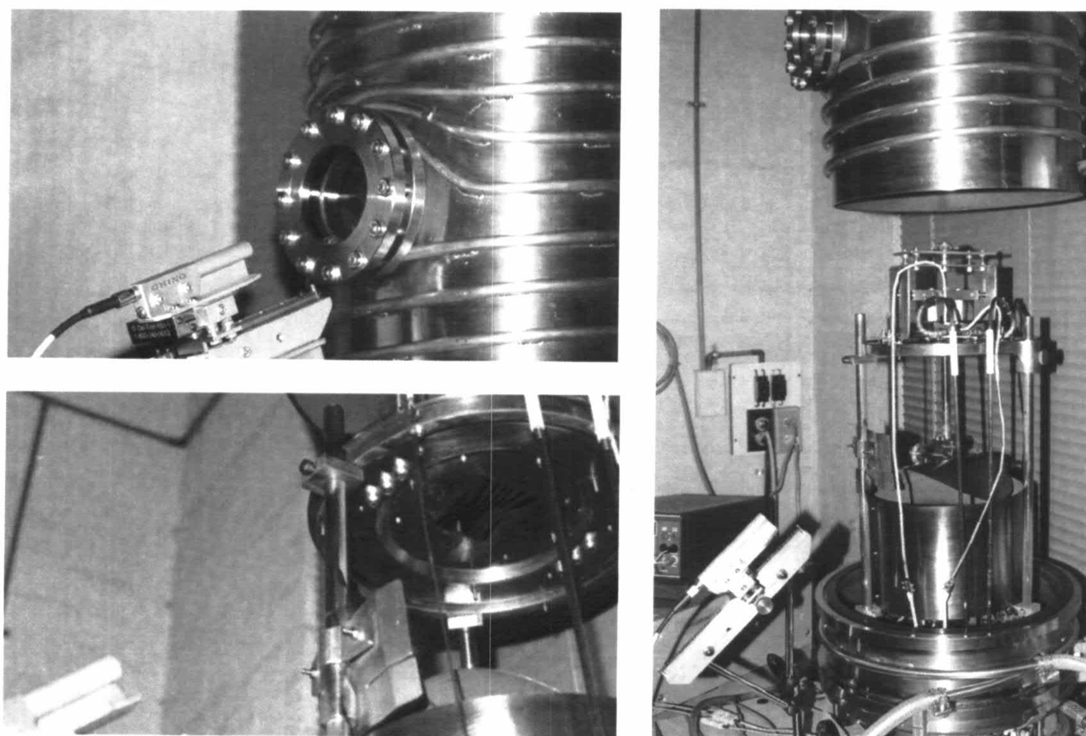

Figure 3.18: Photographs of the pyrometer.

Normally, emissivity (ε) is defined as the ratio of the energy radiated by an object at a given temperature to the energy emitted by a perfect radiator, or

blackbody, at the same temperature. The emissivity of a blackbody is 1.0. All values of emissivity fall between 0.0 to 1.0. Reflectivity (R) is a measure of an object's ability to reflect infrared energy. Transmissivity (T) is a measure of an object's ability to transmit infrared energy. Both R and T are related to emissivity. All radiation energy must be emitted (E), transmitted or reflected, depending upon the temperature of the body. The total energy; the sum of emissivity, transmissivity and reflectivity, is equal to 1. Most objects are not perfect radiators, but will reflect and/or transmit a portion of the energy. Most instruments also have the ability to compensate for different emissivity values, for different materials [47].

To determine the emissivity of our material, we heated the Mo/SLG substrate to a certain temperature measured by using the backside thermocouple. The temperature at the surface of the substrate was measured by using the pyrometer. We then adjusted the emissivity of the pyrometer until it displayed the same temperature as the backside thermocouple. In this experimental set-up, the value of emissivity was approximately 0.107.